THE JOURNAL OF PHYSICAL CHEMISTRY C
A JOURNAL OF THE AMERICAN CHEMICAL SOCIETY

pubs.acs.org/JPCC

Article

Impact of Non-Arrhenius Temperature Behavior on the Fast-Charging Capabilities of $LiCoO_2$–Graphite Lithium-Ion Batteries

Published as part of The Journal of Physical Chemistry virtual special issue "Emily A. Carter Festschrift".

Wesley Chang,[▽] Clement Bommier,[▽] Robert Mohr, and Daniel Steingart*

Cite This: https://dx.doi.org/10.1021/acs.jpcc.0c09972

Read Online

ACCESS | Metrics & More | Article Recommendations

ABSTRACT: Fast-charging lithium-ion batteries in 15 min or less is an important capability that may lead to greater electric vehicle adoption but remains challenging to implement. Heating to moderate temperature (40–50 °C) during the fast-charge step has been introduced as one method to mitigate the loss of lithium inventory by enhancing transport and kinetics. Unfortunately, this edge has two sides as even moderate temperature elevation will accelerate capacity fade due to interface and electrolyte degradation. While the thermal enhancement of transport and degradation is intuitive, the mechanistic effects of various temperature ranges on fast-charging capabilities are under-reported. The present work examines the balance between aging, temperature, and charge rate and describes cycling protocols in combination with high-temperature ranges that may enable fast-charging capabilities. A galvanostatic intermittent titration technique (GITT) analysis reveals non-Arrhenius diffusion behavior at the cell level. This shift is attributed to a mechanistic difference in graphite staging at temperatures above and below 40 °C. Coupled with differential capacity and voltage analysis, we indicate the specific phase transition that is kinetically sluggish at low temperatures relative to the other phase transitions but is comparable to the other phase transitions at high temperatures. This reduction of the transport bottleneck, in addition to the benefits of thermal activation of diffusion, further minimizes the likelihood of lithium plating that is triggered by particle scale transport challenges well before full lithiation of the graphite. This helps to explain recently described outsized successes of elevated temperature fast-charge protocols, but also questions the temperature at which fast-charge should take place, as the diffusivity gains for 55 vs 45 °C are less dramatic than 45 vs 35 °C, and side reactions may deter operation above 50 °C. These diffusivity studies are connected with long-term aging studies which indicate improved high-temperature aging at lower states-of-charge rather than higher states-of-charge. Taken together, we introduce a cycling protocol utilizing a constant current fast-charge at high temperature to take advantage of lower overpotentials, shorter duration at high states-of-charge, and improved cell diffusivity.

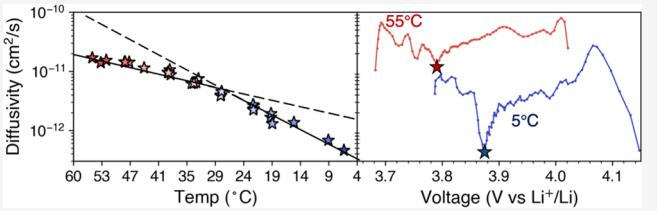

1. INTRODUCTION

The global adoption of electric vehicles, and the hypothesis that 200 mile range alleviates "range anxiety," has led to an interest in fast-charge capabilities comparable with combustion engine vehicles.[1,2] Such fast-charge capability may offset the capital and mass requirements for 300 mile or more batteries. Reports from the calendar year 2017 indicated that the electric vehicle market comprised around 1.7% of global vehicles sold.[3] Recently, the 2020 Bloomberg New Energy Finance Executive Summary concluded that electric vehicles accounted for 3% of global car sales, rising to 7% in 2023.[4] In addition to the cost metric of less than $100/kWh and the cycle life retention of 80% at 1000 cycles,[5] electric vehicle lithium ion batteries (LIBs) should be recharged in 10–15 min to be competitive with conventional combustion engine vehicles.[6] The 15 min fast-charge has been a target set by various government agencies as well as automobile corporations. However, introducing fast-charging capabilities into LIBs imposes significant constraints. Conventional graphite negative electrodes plate lithium at low temperatures and/or high current rates.[7,8] For example, external temperature environments and varying cycling protocols[5] have been introduced as possible methods for mitigating lithium plating and meeting fast-charging specifications. In particular, Wang et al. recently demonstrated the use of a 6C charging rate to 80% state-of-charge (SOC) with 80% capacity retention over 1700 cycles, using asymmetrical temperature modulation.[9] Their large-format electric vehicle pouch cells were selectively heated upon the fast-charging step and then cooled during the discharge

Received: November 4, 2020
Revised: December 17, 2020

step. It is likely that asymmetric heating protocols are concurrently being adopted by various electric vehicle companies in attempts to reduce charge time.

Herein, we provide a mechanistic hypothesis to explain the outsized impact a moderate increase in temperature has on the ability for a "standard" LIB to accept higher charge rates. The use of high temperatures and fast-charging marks a departure from previously established LIB cycling protocols, which stipulated that higher temperatures (>45 °C) should be avoided due to degradation reactions resulting in low cycle life. For example, Popov et al.[10] demonstrated in $LiCoO_2$ (LCO)-based 18650 cylindrical cells 70% capacity loss after 490 cycles at 55 °C in contrast with 30% capacity loss at room temperature and 36% capacity loss at 45 °C. Dubarry et al.[11] reviewed many of these previous studies, concluding that LCO/graphite-based chemistries undergo rapid capacity degradation at high temperatures along with high or medium SOC. These results were further supported by Pecht et al. who reported faster degradation in LCO-based 18650 cylindrical cells at higher temperatures.[12] At the same time, low temperatures also induce capacity fading due to higher anode polarization leading to dendritic lithium deposition. Fast-charging at low temperatures would aggravate lithium deposition even further.

In this manuscript, we first explore the high-temperature fast-charging cycling protocol as recently introduced by Wang et al.[9,13] by comparing the constant current (CC) and constant voltage (CV) contributions in a constant current constant voltage (CCCV) charge protocol. After verifying the benefits of high temperatures to capacity retention, we then conduct a long-term aging study to investigate the effects of both high temperatures and high SOCs. Given the significant impact of temperature on transport, we then conduct diffusivity measurements of LCO/graphite pouch cells using the galvanostatic intermittent titration technique (GITT). We extract an effective diffusivity curve of the full cell as a function of temperature, to explore the relationship between full cell diffusivity, SOC, and temperature. The full cell diffusivity measurements are confirmed to be indicative of graphite anode staging through half-cell GITT measurements and differential voltage analysis. We explain why these results suggest the benefits of high temperature during fast-charging and how higher temperature environments can be utilized while also minimizing increased aging effects. Lastly, we take these aging and steady-state diffusivity studies and demonstrate significantly improved rate capability and fast-charge cycling performance of full cells by avoiding conditions that involve both high temperature and high SOC at the same time.

2. EXPERIMENTAL METHODS

2.1. Pouch Cell Properties. Cells used for cycling/aging tests and initial GITT studies were LCO/graphite pouch cells (nominal capacity of 210 mAh, size 651 628, obtained from AA Portable Power Corp). LCO electrodes were sonicated in *n*-methyl-2-pyrrolidone (NMP), and graphite electrodes were sonicated in deionized water; the respective slurries were dried in the vacuum oven at 150 °C overnight to obtain the dried powder for loading and density measurements. Cells are manufacturer rated to 2C cycling rates.

Additional GITT and fast-charging protocol tests were conducted on 400 mAh LCO/graphite from Li-Fun Technology Co., Ltd. (size 482 727 pouch cells, Zhuzhou City, China). The cathode was pure LCO. Electrolyte was 1 M hexafluorophosphate ($LiPF_6$) in ethylene carbonate (EC), propylene carbonate (PC), diethylcarbonate (DEC) (1:1:1% v/v) with ∼2% fluoroethylene carbonate (FEC), and 1,3-propane sultone (PS) additives. No other additives or coatings were present in the electrodes or the electrolyte. Cells are manufacturer rated to 1C cycling rates. Cell properties are listed in Table 1. Loading and estimated nominal capacity values are per coated area (cm^2).

Table 1. Cell Properties

	210 mAh LCO/graphite (AA portable power)		400 mAh LCO/graphite (Li-Fun Technology Co., Ltd.)	
electrode	$LiCoO_2$	graphite (type unknown)	$LiCoO_2$	graphite (artificial)
loading (mg/cm^2)	17.9 (est.)	14.0 (est.)	20.0	10.2
density (g/cm^3)	1.54 (est.)	1.06 (est.)	4.05	1.6
electrolyte	1 M $LiPF_6$ in EC/DMC (1:1% v/v)		1 M $LiPF_6$ in EC/PC/DEC (1:1:1% v/v), ∼2% FEC and PS	
active material loading	unknown	unknown	98.5%	95%
nominal capacity (mAh/cm^2)	2.68 (est.)	4.8 (est.)	3.0	3.5
other additive/coatings	unknown	unknown	none	none

2.2. Cycling Protocol. Cells were cycled on a Neware BTS4000 cycler, with the described charge protocol and constant current discharge. The lower current cutoff for CCCV charge protocols was C/10. The voltage cutoffs were 4.2 and 2.7 V. Cells were cycled in environmental temperature chambers, with environmental temperature monitored by temperature sensors and cell surface temperatures by thermistors coupled with the cycler with 0.1 °C resolution.

Half-cells were assembled from individual electrodes harvested from the commercial LCO/graphite pouch cells inside an argon-filled glovebox (O_2 < 0.5 ppm, H_2O < 0.5 ppm). Typically, 1.27 cm diameter electrode disks were punched out and placed into flooded 2032-coin cells using dual glass fiber (Whatman), polypropylene (Celgard) separators, 1 M $LiPF_6$ in ethylene carbonate (EC), dimethyl carbonate (DMC) (1:1% v/v) electrolyte (Sigma-Aldrich), and a 750 μm thick Li metal counter electrode (Sigma-Aldrich). Half-cells were cycled at 1 mA using cutoff voltages of 0.01−2.0 V for the anode and 3.2−4.5 V for the cathode, with cutoff voltages in reference to Li^+/Li.

2.3. GITT Protocol. Galvanostatic intermittent titration testing (GITT) was conducted with 10 min current pulses at C/10 followed by a 60 min rest at open circuit potential. The half-cell GITT tests followed the same timing with a 0.1 mA pulse current. For accurate measurement of the diffusivity, only the square root time dependence portion of the transient current pulse was used. This was found by taking a linear regression of the transient pulse to find the slope of best fit, with best fit judged by the mean squared error which was $<1 \times 10^{-4}$ for all temperature conditions. A slightly higher error was found for the lower-temperature regimes because of the increase in the transition time before the square root dependence takes hold. The molar volume and molar mass of LCO and graphite were used for the electrode parameters in calculating the diffusivity. The active material surface area was estimated using Brunauer−Emmett−Teller (Micromeritics ASAP 2020 HV BET analyzer)

https://dx.doi.org/10.1021/acs.jpcc.0c09972
J. Phys. Chem. C XXXX, XXX, XXX−XXX

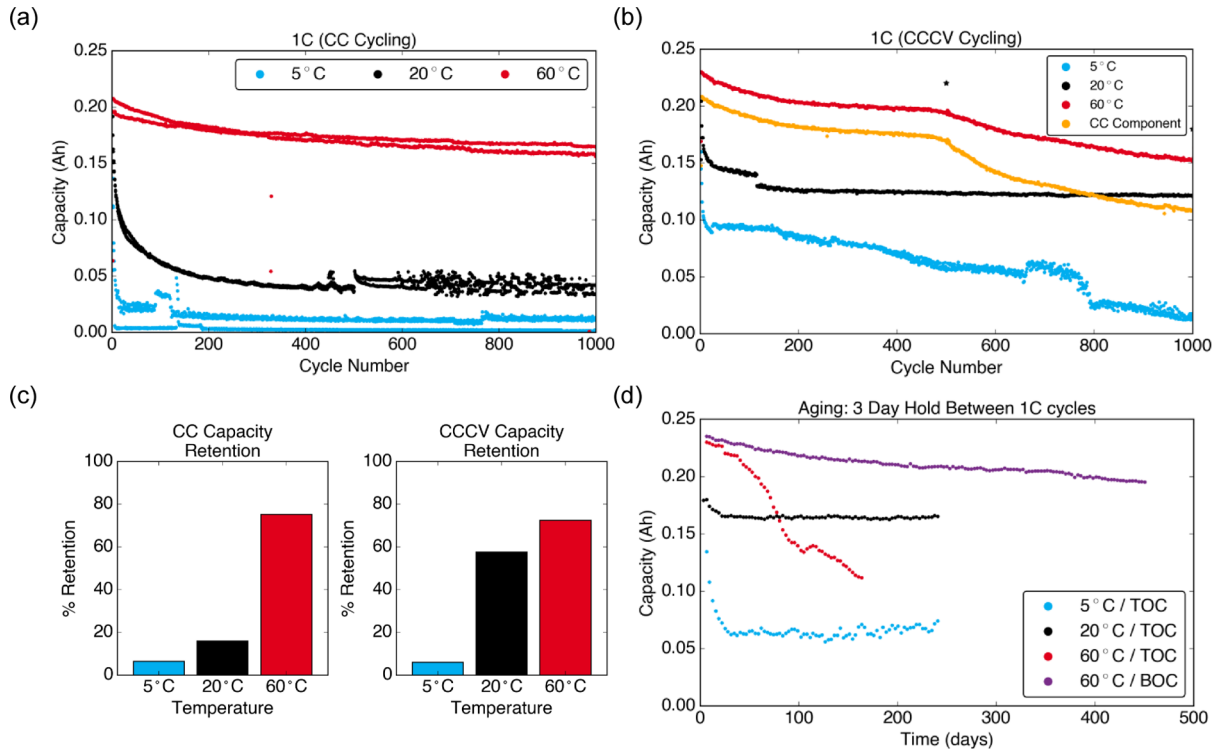

Figure 1. Long-term cycling protocol and aging tests. (a) Charge capacity (Ah) fade of 210 mAh commercial LCO/graphite pouch cells (rated for 2C) at constant current (CC) 1C rate and temperature conditions of 5, 20, and 60 °C. (b) Charge capacity (Ah) fade of 210 mAh commercial LCO/graphite pouch cells at constant current constant voltage (CCCV) 1C rate and the same temperature conditions as (a). CC component of 60°C is depicted in orange, showing faster degradation than the CC cycling protocol in (a). The * for 60 °C at cycle 500 indicates a brief pause before restarting the cycling script, which may have introduced a cycling artifact and kink in the aging rate. (c) Capacity retention at 1000 cycles from the CC and CCCV cycling protocols, showing poor capacity retention (<10%) for both protocols at 5 °C, significantly poorer retention for CC if conducted at 20 °C (15% for CC vs 60% for CCCV), and slightly improved retention for CC (75% for CC vs 70% for CCCV) if conducted at 60 °C. (d) Aging test for cells at 5, 20, and 60 °C at either top-of-charge (TOC) or bottom-of-charge (BOC), with a 72 h hold in between each 1C rate cycle.

measurements from the sonicated and dried electrode material (2.45 m^2/g for LCO, 3.18 m^2/g for graphite).

3. RESULTS AND DISCUSSION

3.1. Comparing Capacity Loss between Constant Current and Constant Current Constant Voltage. The comparison of constant current (CC) and constant current constant voltage (CCCV) charging protocols for cycling at a rate of 1C and three different temperature regimes is shown in Figure 1. For either the CC or CCCV protocol, the low temperature of 5 °C results in poor capacity retention at the rate of 1C (Figure 1a,b). This is attributed to the loss of lithium inventory due to lithium plating at high rates and low temperatures, as is well established in the literature.[14−17] A full investigation of the effects of temperature and current rate on the degree of plating for the cells used in this study can be found in our recent manuscript using the in operando acoustic technique.[8] The capacity retention for a given cell as shown in Figure 1c and described in this section is defined as the charge capacity measured at 1000 cycles vs the initial charge capacity. The high cell overpotential at 1C rate and 20 °C causes the constant current voltage to hit the cutoff of 4.2 V fairly quickly. This limits the capacity obtained and results in only 15% capacity retention of the initial capacity after 1000 cycles. On the other hand, the CCCV charge protocol results in 60% capacity retention of the initial capacity after 1000 cycles. Including a constant voltage portion allows the cell to access additional capacity and reach higher states-of-charge, and this is why conventional cycling tests utilize a CCCV protocol. In contrast, the 60 °C environment results in lower overpotentials, leading to comparable capacity retention between the CC and CCCV charge protocols (Figure 1c).

A closer analysis of the CCCV charge protocol shown in Figure 1b provides informative detail about the relationship between time spent at the high voltage and capacity retention at a given temperature. Decoupling the CC and CV contributions to the total charge capacity at 60 °C reveals that over 90% of the initial capacity is obtained through the CC contribution at the beginning of cycling (orange markers indicate the CC component of the CCCV protocol at 60 °C). After 1000 cycles, the CC contribution drops to merely 47% of the initial capacity, whereas the CC charge protocol in Figure 1a still retains 75% of its initial capacity. The high rate capability of the CCCV protocol is compromised by the CV component during cycling. Whereas the CC protocol begins discharge immediately after the 4.2 V cutoff, the CCCV protocol begins discharge much later due to the longer CV step, during which the cell remains at high SOC until the trickle current cutoff of C/10.

3.2. Long-Term Aging Tests at High-Temperature and Varying SOCs. To further understand and confirm the deleterious effects of high SOC and high-temperature combinations, a long-term aging test was conducted for a total duration of nearly 1.5 years. Cells were cycled at 1C and CCCV charge with 72 h duration rest states in between each cycle and held at either top-of-charge (TOC) or bottom-of-charge (BOC). The results of this aging experiment are depicted in

https://dx.doi.org/10.1021/acs.jpcc.0c09972
J. Phys. Chem. C XXXX, XXX, XXX−XXX

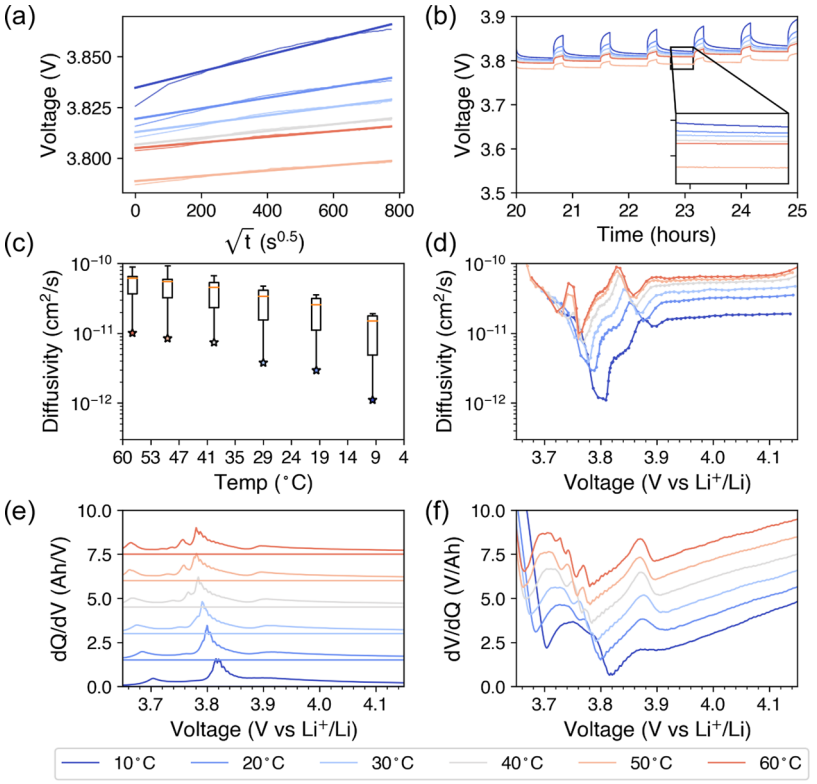

Figure 2. GITT and differential analysis for 210 mAh LCO/graphite commercial pouch cells (AA Portable Power). (a) Linear regression fit of transient voltage vs square root of time during a sample current pulse; note that the lowest temperature condition has a noticeable period of time before entering the square root time dependence. (b) Sample current pulses along with subsequent voltage relaxation steps. (c) Box-and-whisker plot of Arrhenius relation (logarithmic diffusivity and inverse temperature), showing median and confidence interval, with absolute minimum indicated by the starred marker, which indicates the zenith of the diffusivity trough at around 3.8 V. The relationship appears non-Arrhenius, with a steeper drop-off of diffusivity below 40 °C. (d) Diffusivity curves from GITT for all temperature conditions. (e) dQ/dV (Ah/V) of the initial C/20 cycle immediately prior to the GITT charge test for all temperatures. (f) dV/dQ (V/Ah) of the initial C/20 cycle immediately prior to the GITT charge test for all temperatures. Note that differential curves were shifted in the *y*-direction by 1 Ah/V to clearly show each curve.

Figure 1d. After nearly 500 days in a 60 °C environment, the cell held at BOC retained approximately 93% of its initial capacity, showing that even in such a high-temperature environment, capacity losses can be minimized by keeping the cell at lower SOC. In contrast, storing at TOC led to less than 50% retention of initial capacity after only 50 cycles or about 150 days. The high-temperature aged cells can be compared with the lower-temperature aged cells, where although the capacity fade appears to be slower, less capacity is attained due to the lower temperature and higher overpotentials. The significant variation between storage at TOC and BOC at 60 °C is attributed to increased electrolyte degradation when high-temperature storage is paired with high SOC. This echoes findings by Umeda et al.[18] who showed faster onset of a thermal runaway for LCO-type 18650s stored at 80 °C and TOC as opposed to BOC, and by Dahn et al.[19] who showed deleterious effects of higher voltages on overall SOC.

These initial results suggest that reducing time spent at both high SOCs and high temperatures improve capacity retention relative to initial capacity for a 1C cycling rate. At 60 °C, a constant current charge to the voltage cutoff results in about the same capacity as a CCCV protocol, but with a substantially improved cycle life, and could be an effective fast-charge protocol. After the informative, albeit lengthy, 500-day experiment showing that cells stored at lower SOCs age slower than cells stored at higher SOCs and 60 °C, we sought to further explore transport properties of the graphite anode, which is also highly dependent on temperature. While graphite anode transport and diffusivity at higher temperatures have been explored in the past, the recent emergence of fast-charge applications and temperature-dependent properties warrants a closer analysis of the diffusivity curves and how they relate to high-temperature fast-charge conditions. Here, we use GITT to measure the diffusivity of both full cells and half-cells to demonstrate a link between the effective full cell diffusivity and individual electrode diffusivities.

3.3. Analysis of Effective Diffusivity as Measured by GITT. The GITT measurements were conducted according to Weppner's original 1977 paper,[21] where short pulse galvanostatic titration experiments result in a constant equilibrium voltage, leading to the following equation

$$D = \frac{4}{\pi}\left(\frac{m_B V_M}{M_B S}\right)^2\left(\frac{\Delta E_s}{\tau \times (dE/d\sqrt{t})}\right)^2$$

where τ is the current pulse duration, m_B is the electrode mass, V_M is the molar volume, M_B is the molar mass, S is the electrochemically active surface area, ΔE_s is the steady-state voltage change assuming a sufficiently low current pulse, and $dE/d\sqrt{t}$ is the slope of the square root time-dependent current pulse. This relation is derived from the solution to Fick's second law equation assuming certain boundary conditions, with the square root time dependence arising from the assumption of short-time current pulses ($t \ll L^2/D$).

https://dx.doi.org/10.1021/acs.jpcc.0c09972
J. Phys. Chem. C XXXX, XXX, XXX−XXX

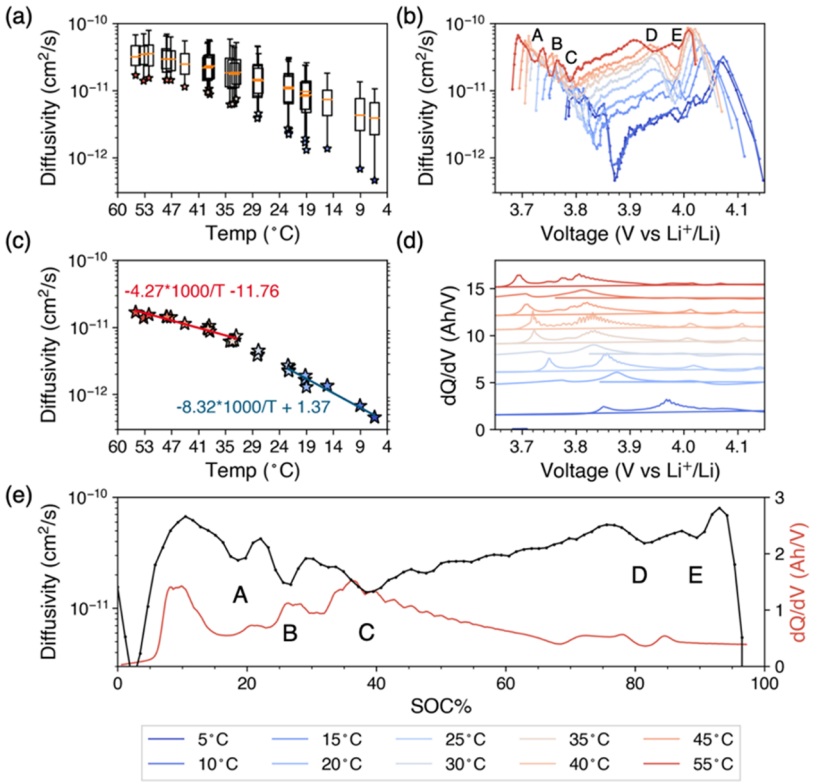

Figure 3. GITT and differential capacity analysis for 400 mAh Li-Fun LCO/graphite pouch cells (Li-Fun). Multiple cells were tested at each temperature condition, with temperature monitored by thermistors on the pouch cell surface. (a) Box-and-whisker plot of Arrhenius relation (logarithmic diffusivity and inverse temperature), showing median and confidence interval. The median diffusivity appears linear and Arrhenius, whereas the minimum diffusivity appears non-Arrhenius. (b) Diffusivity curves from GITT of all cells tested, with local minima labeled A−E. Note the significantly depressed diffusivity trough for point C (stage 2L/2) at lower temperatures. (c) Calculated activation energies from linear fit trendlines for the primary diffusivity trough located at near 3.8 V for the two different temperature regimes, indicating a doubling of the activation energy from high to low temperatures. (d) Corresponding dQ/dV of C/10 constant current cycle immediately prior to GITT, with peaks corresponding to graphite two-phase regions and also correlated with GITT diffusivity troughs. Note that the differential peaks in (d) were shifted in the y-direction by 1 Ah/V to clearly show the trends in each individual curve. (e) Comparison of the diffusivity curve and dQ/dV for a cell at 55 °C showing the correlation of diffusivity minima with dQ/dV peaks.

While GITT tests are conventionally conducted on half-cells[20,21] to investigate the diffusivity of one electrode in reference to a lithium metal reference, a recent study by Cabañero et al.[22] suggested that the full cell GITT diffusivity values could be attributed mainly to the graphite electrode at lower SOCs and to the cathode at higher SOCs due to the differences between the two voltage profiles at lower and higher SOCs. Dees et al. showed that diffusivity values of the graphite anode should agree within an order of magnitude,[20] and many published reports appear to measure relatively similar values,[22] with differences arising from the measurement of electrochemical surface area. As explained in the next section, individual measurements of anode and cathode half-cells suggest that the diffusion troughs observed in full cell effective diffusivity curves can be matched to the graphite anode half-cells as well as the graphite phase transition peaks in differential analysis.

GITT was conducted on the 210 mAh pouch cells in temperature environments ranging from 0 to 60 °C in 10 °C increments, where temperature sensors of the cell surface showed that the surface temperature did not deviate much from the environmental temperature. This is because the current pulses use a low rate of C/10 and have a short duration of 10 min, as consistent with other GITT reports elsewhere. The square root time dependence of the galvanostatic current pulse was found by implementing a linear regression vs the square root of time (Figure 2a). Lower temperatures were observed to have a longer transition period (~100 s for the 0 °C condition) before entering the square root time-dependent relationship. The subsequent relaxation step was confirmed to be of adequate duration for the cell to reach near steady state, with changes in the voltage being negligible or on the order of noise (<1 mV/h), as shown in Figure 2b. The Arrhenius plot of logarithmic diffusivity and the inverse temperature are plotted in Figure 2c, where the relationship between the full cell diffusivity and temperature deviates from linearity. The box-and-whisker plot shows the spread of diffusivity, including the median and confidence interval, with the starred markers indicating the minimum diffusivity value that corresponds to the primary diffusion trough around 3.8 V. The slope of the Arrhenius plot decreases at higher temperatures, indicating a possible change in the activation energy (Figure 2c). Note that the calculated diffusivity measurements here are within the same range of 10^{-9}−10^{-11} cm^2/s for the graphite diffusivity in prior studies.[23,24] The diffusivity curves as a function of voltage are shown in Figure 2d, where the primary diffusion trough is observed at 3.8 V along with several minor troughs at higher SOCs. These correlate with the peaks observed in differential analysis (Figure 2e,f), which correspond to graphite phase transitions. Interestingly, the differential analysis indicates extra peaks at temperatures above 40 °C, notably between 3.75 and

https://dx.doi.org/10.1021/acs.jpcc.0c09972
J. Phys. Chem. C XXXX, XXX, XXX−XXX

3.8 V. A closer investigation of the diffusivity curves in Figure 2d shows that the extra peak immediately below 3.8 V as seen in Figure 2e seems to also arise in the diffusivity curve. A similar curvature of the Arrhenius plot was observed in a larger format 1500 mAh pouch cell from the same supplier (AA Portable Power), shown in Figure 4a.

To confirm the trends extracted from commercial cells with proprietary additive compositions, we applied the same GITT study at varying temperatures between 5 and 55 °C with a LCO/graphite pouch cell (nominal capacity of 400 mAh, pure LCO, artificial graphite) manufactured with known compositions. The manufacturer of these cells (Li-Fun Technology Co., Ltd., Zuzhou City, China) has been extensively tried and tested by the Dahn research group. The tested batch of cells use pure LCO without surface coatings as the cathode, artificial graphite as the anode, and 1 M $LiPF_6$ in EC/DEC/PC (1:1:1% v/v) with ∼2% FEC and PS, which improve capacity retention at 55 °C cycling as investigated by Lucht et al.[25] Both FEC and PS result in lower impedance and alter the composition of the solid−electrolyte interphase (SEI), with PS resulting in lithium alkylsulfonate formation and inhibition of ethylene gassing. The use of a known temperature-stable electrolyte composition along with pure LCO and a high manufacturer-rated voltage cutoff of 4.35 V allows for a diffusivity study without significant degradation effects conflating the results. The GITT results confirmed the non-Arrhenius trend observed for commercial cells as in Figure 2. For improved fidelity, three cells were tested at 10 different temperatures, in increments of 5 °C instead of 10 °C. The measured pouch cell surface temperature was plotted against the measured diffusivity. The $dE/d\sqrt{t}$ term was accurately measured by fitting a linear regression line to the square root time dependence in the transient pulse, and the ΔE_s term was found by taking the average steady-state voltage during the relaxation step.

The GITT results confirm that higher temperatures increase diffusivity at all states-of-charge (Figure 3b). This is especially apparent with the large diffusion trough present at lower temperatures between 3.85 and 3.90 V (point C). The correlation of diffusion troughs with peaks in differential analysis and graphite stage transitions was first explored by Dahn and Aurbach.[24,26] Lithiation of the initial dilute solid solution (stage 1L, $x \sim 0.04-0.07$) results in stage 4L ($x \sim 0.12$) at around 3.7 V, followed closely by stage 3L ($x \sim 0.21$), to a liquidlike stage 2L phase, to stage 2 ($x \sim 0.5$), and finally stage 1 at high SOC.[26,27] Comparing these initial results to our study, we find that the main diffusion trough at around 3.85 V or 35% SOC (point C) can be assigned to the stage 2L/2 transition. The magnitude of this trough increases by over an order of magnitude with higher temperatures, from around 7×10^{-13} cm^2/s at 5 °C to 1×10^{-11} cm^2/s at 55 °C.

The diffusivity troughs in Figure 3b can be further compared with dQ/dV peaks in Figure 3d. At 55 °C, there are three similarly sized diffusivity troughs at low states of lithiation (points A−C) assigned to stage 4L/3L, stage 3L/2L, and stage 2L/2 phase transitions. The dQ/dV curves in Figure 3d show three peaks that are present at high temperatures but absent at low temperatures, as also reported by Aurbach.[28] dQ/dV peaks indicate two-phase regions of graphite staging. At 5 °C, we still observe point A and point B in the diffusivity curves, with point C exhibiting a significantly lower diffusivity. This suggests that lower temperatures hinder the staging process through these phases and may be why only one large differential capacitance peak is observed at lower temperatures. At higher SOCs, we attribute point D to a LCO phase change and point E to the stage 2/1 transition. Lastly, there is less variability in diffusivity across all SOCs at higher temperatures. The 55 °C condition ranges between 1×10^{-11} and 4×10^{-11} cm^2/s, as opposed to $7 \times 10^{-13}-1 \times 10^{-11}$ cm^2/s at 5 °C.

Figure 3a indicates that the median diffusivity, as plotted by a box-and-whisker plot, is roughly linear. The linear logarithmic diffusivity vs inverse temperature trend indicates Arrhenius behavior of the overall diffusivity, with a single activation energy at any given temperature. However, we note an interesting deviation from this linearity with the minimum diffusivity. The minimum diffusivity exhibits a clear non-Arrhenius trend (Figure 3c). The higher temperatures above 40 °C follow a linear fit that has a lower slope than the lower temperatures below 40 °C. This suggests two different activation energies, with the lower-temperature regime measuring twice the activation energy for the stage 2L/2 transition. Therefore, there is a fundamental change in the diffusion mechanism of graphite staging here, with higher temperature significantly reducing the diffusivity bottleneck that is present at colder temperatures. While several recent studies present Arrhenius behavior between diffusivity and temperature, those studies were generally conducted up to 30 °C and no higher, which is probably why this nonlinear regime was not observed.[22] The non-Arrhenius trend shown here is reminiscent of earlier reports by Aurbach et al.[27,28] describing a non-Arrhenius diffusivity trend with measurements up to 80 °C, where those studies were conducted using the potentiostatic intermittent titration technique (PITT) and explained with a lattice gas model. However, galvanostatic pulses rather than potentiostatic generally have improved fidelity especially within the graphite phase transitions that occur fast in a small range of differential capacities. Aurbach claimed that this temperature-dependent diffusion barrier may stem from a change in the type of short-range interactions of the intercalated lithium ions.

Why do the recent demonstrations[9] of fast-charging at high temperatures work so well, despite the increase in electrolyte degradation that occurs in conventional carbonate-based electrolytes? We show that significant diffusivity bottlenecks within stage 2L/2 are alleviated as temperature changes from 25 °C to just above 40 °C, thereby mitigating the chance for lithium plating. The location of the stage 2L/2 diffusivity trough is at the lowest point of the entire diffusivity curve, at around 3.8 V or 30% SOC. After approximately 45 °C, the benefits of increased temperature are less dramatic due to the trends outlined in this work. This is also where recent work has demonstrated plating may begin to occur during 2C or higher charge rates. For example, Konz et al.[29] observed plating signatures at rates higher than 2C with differential open-circuit voltage (OCV) at around 50% SOC and an increase in graphite SEI resistance at around 30% SOC. Bommier et al.[8] observed a reversal in the acoustic time-of-flight shift when plating occurs, generally around 30% SOC. The exact location of the time-of-flight shift, which is a function of cell thickness and modulus changes, depends on rate and temperature. Fear et al.[30] observed with graphite half-cells a consistent voltage minimum near 45% SOC attributed to lithium plating at 0 °C. They conducted optical microscopy showing localized plating occurring between 20 and 40% SOC. These studies are all in agreement with the onset of plating occurring at the stage 2L/2 diffusivity bottleneck. In agreement with these studies, the diffusivity curves for both types of cells and a third type are replotted as a function of SOC% in Figure 4b−d, which all show that this minimum diffusivity is located

https://dx.doi.org/10.1021/acs.jpcc.0c09972
J. Phys. Chem. C XXXX, XXX, XXX−XXX

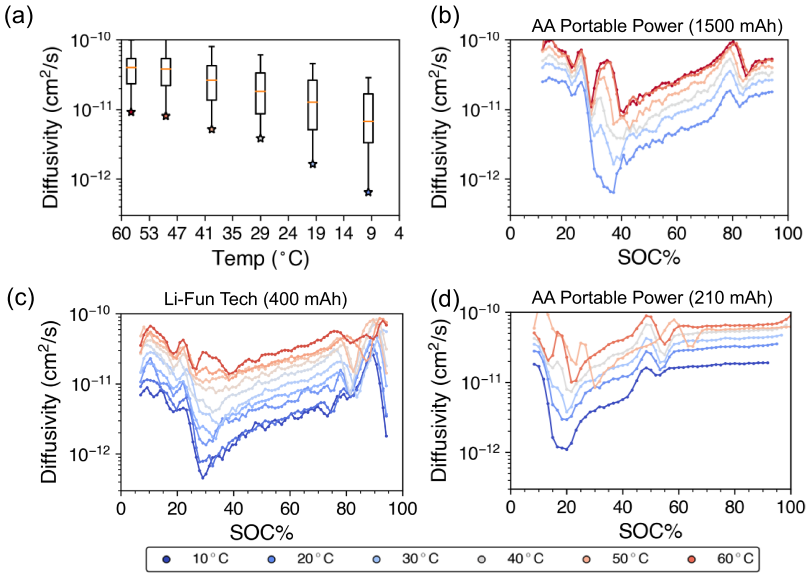

Figure 4. Minimum diffusivity between 20 and 40% state-of-charge. (a) Arrhenius plot and (b) diffusivity curve from GITT of larger LCO/graphite pouch cells (1500 mAh, AA Portable Power), showing the non-Arrhenius trend of the minimum diffusivity. Diffusivity curves replotted as a function of state-of-charge normalized to that of the cold temperature charge endpoint capacity, showing that the minimum diffusivity occurs between 20 and 40% SOC for all cell types and temperatures tested: (c) Li-Fun Tech 400 mAh pouch cells and (d) AA Portable Power 210 mAh pouch cells.

between 20 and 40% SOC. Slight variations may be due to varying degrees of normalization of the state-of-charge and slight differences in chemistry in the commercial cells that would alter the charge endpoint capacity at the voltage cutoff.

In combination with our initial cycling protocol studies which indicated the decreased aging rate of cells stored for 1.5 years at lower SOCs as opposed to higher SOCs, we can take advantage of certain fast-charging protocols to avoid both high SOC and high-temperature conditions. For example, we showed that a constant current charge at 60 °C results in nearly the same capacity as a constant current constant voltage charge, due to the lower overpotentials at 60 °C. A constant current charge also avoids time spent at the high SOC as in a constant voltage protocol and would delay the degradation observed at those conditions. To further minimize duration spent at both high temperature and high SOC, the cells can be selectively heated immediately prior to and during the charge step. Since a constant current fast-charge of 2C occurs in less than 30 min (or a fast-charge of 5C which would occur in less than 12 min), the duration of time spent at high temperature would be short. This mechanistic analysis explains why the selective heating protocol as introduced by Wang et al.[9] resulted in significantly improved capacity retention of fast-charged cells.

3.4. Further Investigation of Anode and Cathode Half-Cells. One challenge with GITT studies of full cells is the difficulty in decoupling anode and cathode contributions to the diffusivity. However, a recent study by Cabañero et al.[22] suggested that the lower states-of-charge of a full cell can approximate graphite diffusivities, and the higher states-of-charge the cathode diffusivities. This is primarily because the cathode half-cell has a nearly flat voltage profile at lower states-of-charge, whereas the graphite half-cell voltage profile flattens at the higher voltages. To confirm which electrode contributed more to the diffusivity troughs observed at lower temperatures, both anode and cathode half-cells were made from disassembling the original pouch cells and cycled at a current rate of 1 mA/cm^2. For the graphite half-cells, a steep drop-off in capacity was observed between the 30 and 20 °C increments from ∼3.0 mAh/cm^2 to less than 1 mAh/cm^2 (Figure 5a). This is also the range where the activation energy was observed to change, as observed by the change in the slope of the Arrhenius plot in Figures 2c and 3c. The anodes at 0 °C had negligible capacity and are not included in the plot. For the cathode half-cells, temperature does not drastically affect the capacity, which remains steady at around 3.5 mAh/cm^2 regardless of the temperature (Figure 5b). These half-cell results confirm that the graphite anode exhibits faster capacity fade than the LCO cathode at temperatures of 30 °C or lower and further supports that diffusivity bottlenecks within stages 2L/2 causes this reduction in capacity. The half-cell at 30 °C starts at a high capacity on the first cycle but then experiences a sudden drop in capacity, which may be due to a plating event. The half-cell at 20 °C starts at a low capacity immediately, signaling poor transport at this temperature. These results show that the graphite half-cell experiences greater capacity loss at low temperatures when compared with the LCO half-cell, which further suggests that the graphite anode rate capability is more susceptible than the cathode to diffusivity bottlenecks at lower temperatures.

GITT measurements were then conducted on the half-cells at temperatures of 60−10 °C (Figure 5c,d). For the graphite anode half-cell, the diffusivity curve shows the presence of two major diffusion troughs around 0.08 and 0.11 V vs Li$^+$/Li (Figure 5e). These two troughs are attributed to the stage 2 to stage 1 (point D), and stage 2L to stage 2 (point C) transitions, respectively. In Figure 5g, where the same GITT is plotted as a function of SOC, point C is located between 20 and 40% SOC, which agrees with the full cell diffusivity curves and the prior discussion on plating onset occurring within this range. The minimum diffusivity as calculated from half-cell data may be more difficult to ascertain due to the increased noise observed. The wide trough in Figure 5e at the low state of lithiation at 0.22 V (unlabeled) is attributed to the stage 1L to stage 4L transition. At higher temperatures, two small troughs are observed between 0.14 and 0.17 V vs Li$^+$/Li. The trough at 0.14 V has previously been attributed to the stage 3L to stage 2L transition (point B). The trough at 0.17 V is assigned to the stage 4L to stage 3L transition (point A). These

https://dx.doi.org/10.1021/acs.jpcc.0c09972
J. Phys. Chem. C XXXX, XXX, XXX−XXX

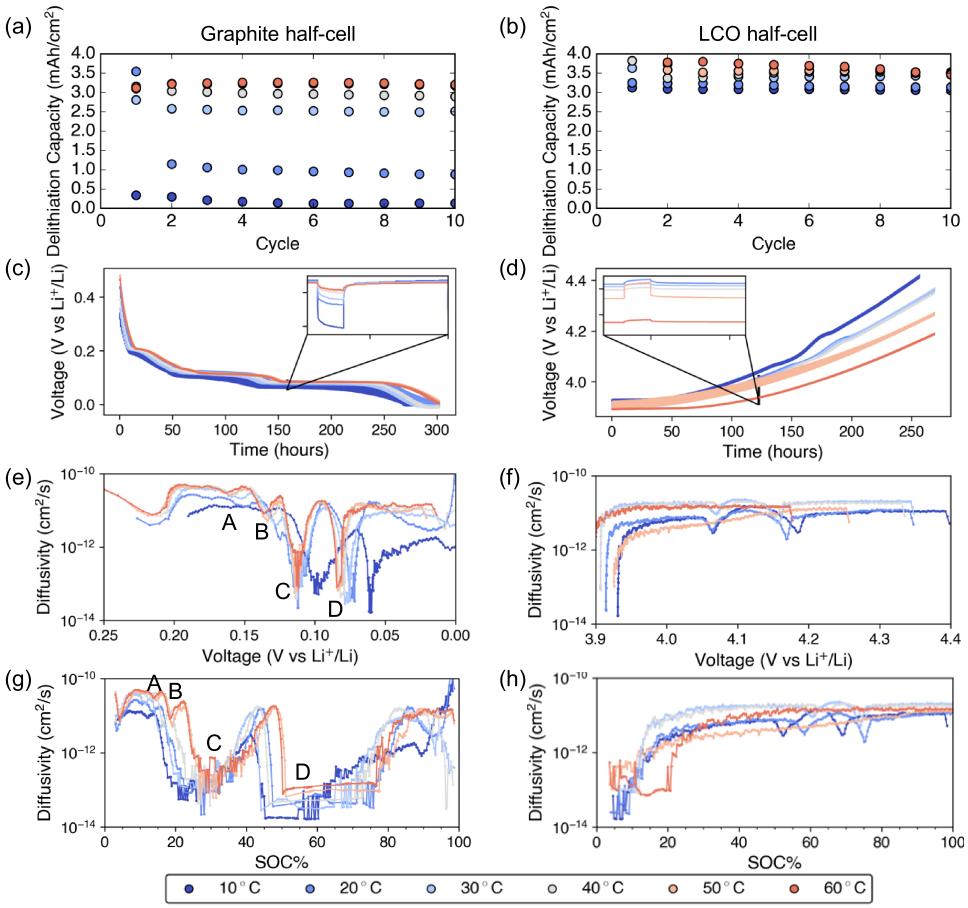

Figure 5. Half-cell capacity and diffusivity measurements. (a) Graphite anode half-cell delithiation capacities (mAh/cm^2) for 10 cycles at a current rate of 1 mA/cm^2 and (b) LCO cathode half-cell delithiation capacities (mAh/cm^2) for 10 cycles at a current rate of 1 mA/cm^2. Graphite half-cell shows low capacities due to diffusivity limitations below 40 °C at the current rate tested, whereas the LCO half-cell is not significantly affected by temperature. (c) GITT protocol for the graphite anode half-cell, with the inset showing a representative transient and relaxation pulse. (d) GITT protocol for the LCO cathode half-cell, with the inset showing a representative transient and relaxation pulse. (e) Diffusivity curve (cm^2/s) for graphite anode half-cell where point A marks stage 4L to 3L, point B marks stage 3L to stage 2L, point C marks stage 2L to stage 2, and point D marks stage 2 to stage 1. (f) Diffusivity curve for LCO cathode half-cell. (g) Diffusivity curve for the graphite anode as a function of SOC, showing that point C (stage 2L/2) corresponds to the primary diffusivity bottleneck in the full cell (Figure 3b) and also occurs between 20 and 40% SOC here. (h) Diffusivity curve for the LCO cathode as a function of SOC, showing two small troughs corresponding to LCO phase transitions at around 50 and 70% SOC.

troughs also correspond to points A and B observed in the full cell GITT (Figure 3b), confirming that the observed diffusivity troughs are primarily due to graphite intercalation bottlenecks rather than cathode effects. Points A and B in both Figure 3b (full cell diffusivity) and Figure 5e (anode diffusivity) are less distinguishable at low temperatures but more noticeable at higher temperatures.

Similarly, GITT was conducted on the cathode half-cells (Figure 5f,h). The diffusivity values are less dependent on temperature, with about 0.5 × 10^{-10} cm^2/s difference in the endpoints. As expected, there are no significant diffusivity troughs with temperature, with the diffusivity profile being nearly flat through the entire range of charge. The minor troughs at around 4.08 and 4.17 V are attributed to several phase transitions of the LCO cathode at high SOCs (~50 and 70% SOC).[31]

3.5. Fast-Charge Cycling Protocol. The GITT results indicate that temperatures above 40 °C significantly change the activation energy of the stage 2L to 2 transition. The half-cell experiments confirm that the bypass of the large diffusivity trough in this region is linked to the significant increase in anode rate capability. The sensitivity of graphite staging to temperature can be determined from the full cell GITT without a three-electrode cell. Taking these mechanistic insights, a proof-of-concept was introduced to demonstrate the improved fast-charging capabilities at higher temperatures while minimizing duration spent at high SOCs. The 210 mAh commercial cell manufacturer rated for 2C was charged at a current rate of 5C using a CC protocol in a 60 °C environment (Figure 6a). A CC protocol instead of a CCCV protocol limits the time spent at the high-voltage cutoff while in the 60 °C environment. As shown earlier, at 60 °C, a CC charge recovers most of the capacity that would be recovered by a CCCV charge and also results in improved capacity retention over cycling. Over 500 cycles of a 4−5 min 5C charge and 1C discharge, the cell was able to reach roughly 30% SOC per cycle. While short of a full charge, this demonstrates the cell could be cycled at a much faster charge than the 2C rating just with simple changes to the cycling protocol. A 5C charge rate showed negligible capacity at room temperature, indicating the significant impact of high-temperature environments on fast-charging capabilities.

The fast-charging high-temperature protocol was replicated for the 400 mAh Li-Fun cells, which were manufacturer rated for 1C. While these cells could not be appreciably charged at rates

https://dx.doi.org/10.1021/acs.jpcc.0c09972
J. Phys. Chem. C XXXX, XXX, XXX−XXX

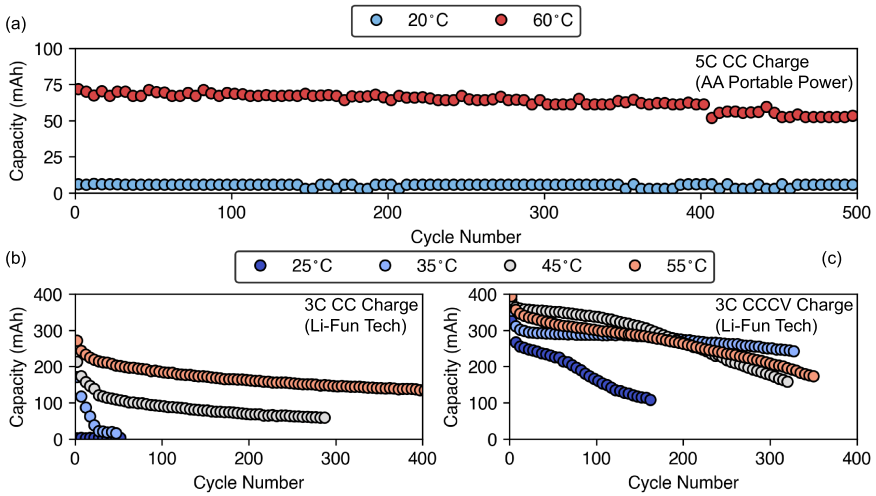

Figure 6. High-temperature fast-charge cycling protocol. (a) Fast-charge protocol of 210 mAh pouch cells (AA Portable Power, rated for 2C) at 5C charge, demonstrating greatly enhanced rate capability at 60 °C over 500 fast-charge cycles. (b) Fast-charge protocol with 400 mAh Li-Fun cells (rated for 1C) at constant current 3C charge demonstrates enhanced capacity retention up to 60% SOC at an elevated temperature of 55 °C. (c) Constant current constant voltage 3C charge demonstrates enhanced capacity retention at 35 °C, but faster capacity fades beyond 35 °C. At 55 °C, the CCCV cell degrades faster than the CC cell despite starting at a higher capacity due to the constant voltage step.

2C or higher at room temperature due to instantly hitting the voltage cutoff of 4.35 V, a temperature environment of 55 °C (with a measured cell surface temperature reaching 60 °C during the fast-charge) allowed the cells to charge at a rate of 3C (Figure 6b). The constant current 3C charge at 55 °C takes about 10 min before hitting the voltage cutoff and attains over 60% SOC during that time. This is not too far from the goal of 80% SOC with a 15 min charge time. With a CCCV charge protocol, the benefits of higher temperatures to capacity retention are not as clear (Figure 6c). The improvement in capacity retention is clear when comparing CC and CCCV charge protocols at low temperatures. However, at 55 °C, the CCCV charged cell has a lower capacity than the CC charged cell after 300 cycles. A CC charge protocol minimizes duration spent at high SOCs, and temperatures above 40 °C result in enhanced cycle life when compared with the CCCV protocol.

The different staging mechanism observed at >40 °C that causes a non-Arrhenius diffusivity trend does not take into account other effects such as fast-charging inhomogeneity and greater SEI decomposition. Fast-charge rates result in significantly higher overpotentials, with buildup of lithiation fronts near the separator side of the graphite electrode and also inhomogeneous staging at the particle level.[32,33] As recently demonstrated by Finegan et al.,[32] a significant lithiation front develops during a 6C charge and only the surface of the graphite electrode nearest the separator underwent any transition to stage 3L or stage 2/2L. As a result of the faster diffusivity at 60 °C, especially within the deep stage 2L/2 trough, the lithiation fronts observed in single particles as well as the entire electrode by Finegan et al. may be overcome more easily, resulting in higher capacities and deeper degrees of lithiation while minimizing plating. In parallel with these electrochemical analyses, Cañas et al.[34] recently demonstrated with in situ X-ray diffraction (XRD) a more homogeneous graphite phase transition process at around 47 °C, with an increased overlap of several different phases. Bauer et al.[35] also demonstrated with dilation measurements that graphite lithiation occurs in a multiphase process at both high current rates and low temperatures. Regarding plating likelihood within or after the stage 2L/2 transition, various measurement techniques including differential OCV analysis,[29] acoustic time-of-flight shifts,[8] and optical microscopy[30] have all pointed toward significant lithium plating to occur between 30 and 50% SOC during 3C and higher fast-charge rates.

While fast-charging presents a situation that is much further from equilibrium than GITT studies, high-temperature fast-charge rates should still reduce graphite anode diffusivity energy barriers. The much greater internal temperature rise due to the fast-charge should be taken into account when controlling the environmental temperature, though this is out of the scope of the current study. This internal temperature rise most likely contributes to observed diffusivity values of high rates that are higher than would be expected by GITT, as recently shown by Dees et al.[36] The <2 Ah pouch cells in the current study measured about 10 °C higher on the surface than the temperature chamber during the fast-charge. For larger >2 Ah-size commercial cells, improved thermal management systems can be used for monitoring the even more significant rise in temperature upon fast-charging and taking advantage of a selective heating protocol to improve diffusivity while minimizing degradation. Future extension of this high-temperature fast-charge mechanism should continue to use high-temperature stable electrolytes[37] that meet the cost and scalability requirements for practical adoption.

4. CONCLUSIONS

In short, we present a diffusivity argument to explain why high-temperature conditions aid the fast-charging capabilities of conventional LCO/graphite pouch cells.

(1) We first demonstrate that the additional capacity extracted from the constant voltage charge step at 25 °C becomes less significant at 60 °C, where CC and CCCV charge protocols retain similar capacities. This suggests the possibility of utilizing a constant current charge protocol at high temperatures to obtain sufficient capacity by taking advantage of lower overpotentials and less time spent at higher states-of-charge. Long-term aging studies over the course of 1.5 years show slower aging rates at 60 °C when stored at bottom-of-charge as compared to top-of-charge.

https://dx.doi.org/10.1021/acs.jpcc.0c09972
J. Phys. Chem. C XXXX, XXX, XXX−XXX

(2) Careful statistically confirmed GITT measurements of different LCO/graphite pouch cells demonstrate a non-Arrhenius relationship between the minimum cell diffusivity and cell temperature. Diffusivity measurements from GITT indicate a change in the diffusion mechanism of the graphite stage 2L to 2 transitions at around 40 °C, as measured by a doubling of the activation energy at lower temperatures. All diffusivity troughs are correlated with differential capacity peaks, where graphite phase transitions occur, though some of the differential capacity peaks are not discernible at low temperatures. GITT and differential analysis are then conducted on individual half-cells to show how full cell diffusivity can be related to the graphite stage transitions. The improvements in the diffusivity of the stage 2L/2 transition around 30% SOC explain why higher temperatures mitigate lithium plating.

(3) This concept of utilizing high temperatures while avoiding time spent at high voltages to bypass graphite diffusivity troughs and minimize electrolyte degradation is then applied to a high-temperature fast-charge protocol. A 3C constant current charge protocol at 55 °C results in over 60% capacity retention in under 15 min, whereas the same cells could not be charged faster than 1C at 25 °C. This approaches the accepted target of 80% SOC in 15 min or less. Over the course of 400 fast-charge cycles at 55 °C, the constant current protocol retains the same capacity as a constant current constant voltage protocol.

These results help to explain some recent demonstrations of effective high-temperature fast-charge protocols both in academia and industry. Proper temperature controls can mitigate unwanted lithium deposition by enhancing cell diffusivity through heating. The non-Arrhenius behavior of graphite lithiation at high temperatures deviates from conventionally understood temperature-dependent phase behavior, and more fundamental mechanistic studies should be undertaken to study the 40−60 °C temperature range for fast-charging lithium-ion batteries.

AUTHOR INFORMATION

Corresponding Author

Daniel Steingart − *Department of Mechanical and Aerospace Engineering, Andlinger Center for Energy and the Environment, and Department of Chemical and Biological Engineering, Princeton University, Princeton, New Jersey 08544, United States; Department of Earth and Environmental Engineering, Department of Chemical Engineering, and Columbia Electrochemical Energy Center, Columbia University, New York 10027, United States;* orcid.org/0000-0002-8184-9641; Email: dan.steingart@columbia.edu

Authors

Wesley Chang − *Department of Mechanical and Aerospace Engineering and Andlinger Center for Energy and the Environment, Princeton University, Princeton, New Jersey 08544, United States; Department of Chemical Engineering and Columbia Electrochemical Energy Center, Columbia University, New York 10027, United States;* orcid.org/0000-0002-9389-1265

Clement Bommier − *Andlinger Center for Energy and the Environment, Princeton University, Princeton, New Jersey 08544, United States; Columbia Electrochemical Energy Center, Columbia University, New York 10027, United States*

Robert Mohr − *Department of Chemical Engineering and Columbia Electrochemical Energy Center, Columbia University, New York 10027, United States*

Complete contact information is available at: https://pubs.acs.org/10.1021/acs.jpcc.0c09972

Author Contributions

[▽]W.C. and C.B. contributed equally to this work.

Notes

The authors declare no competing financial interest.

ACKNOWLEDGMENTS

W.C. and C.B. were supported by Mercedes Benz Research and Development North America. C.B. was supported by the Princeton IP Accelerator Fund. R.M. was supported by a grant from ARPA-E.

REFERENCES

(1) Tomaszewska, A.; Chu, Z.; Feng, X.; O'Kane, S.; Liu, X.; Chen, J.; Ji, C.; Endler, E.; Li, R.; Liu, L.; et al. Lithium-Ion Battery Fast Charging: A Review. *eTransportation* **2019**, *1*, No. 100011.

(2) Schmuch, R.; Wagner, R.; Hörpel, G.; Placke, T.; Winter, M. Performance and Cost of Materials for Lithium-Based Rechargeable Automotive Batteries. *Nature Energy* **2018**, *3*, 267−278.

(3) Yang, X.-G.; Wang, C.-Y. Understanding the Trilemma of Fast Charging, Energy Density and Cycle Life of Lithium-Ion Batteries. *J. Power Sources* **2018**, *402*, 489−498.

(4) BloombergNEF. Bloomberg Electric Vehicle Outlook 2020, 2020. https://efiling.energy.ca.gov/getdocument.aspx?tn=233410.

(5) Mussa, A. S.; Klett, M.; Behm, M.; Lindbergh, G.; Lindström, R. W. Fast-Charging to a Partial State of Charge in Lithium-Ion Batteries: A Comparative Ageing Study. *J. Energy Storage* **2017**, *13*, 325−333.

(6) Keyser, M.; Pesaran, A.; Li, Q.; Santhanagopalan, S.; Smith, K.; Wood, E.; Ahmed, S.; Bloom, I.; Dufek, E.; Shirk, M.; et al. Enabling Fast Charging − Battery Thermal Considerations. *J. Power Sources* **2017**, *367*, 228−236.

(7) Waldmann, T.; Wilka, M.; Kasper, M.; Fleischhammer, M.; Wohlfahrt-Mehrens, M. Temperature Dependent Ageing Mechanisms in Lithium-Ion Batteries − A Post-Mortem Study. *J. Power Sources* **2014**, *262*, 129−135.

(8) Bommier, C.; Chang, W.; Lu, Y.; Yeung, J.; Davies, G.; Mohr, R.; Williams, M.; Steingart, D. In Operando Acoustic Detection of Lithium Metal Plating in Commercial LiCoO2/Graphite Pouch Cells. *Cell Rep. Phys. Sci.* **2020**, *1*, No. 100035.

(9) Yang, X.-G.; Liu, T.; Gao, Y.; Ge, S.; Leng, Y.; Wang, D.; Wang, C.-Y. Asymmetric Temperature Modulation for Extreme Fast Charging of Lithium-Ion Batteries. *Joule* **2019**, *3*, 3002−3019.

(10) Ramadass, P.; Haran, B.; White, R.; Popov, B. N. Capacity Fade of Sony 18650 Cells Cycled at Elevated Temperatures: Part I. Cycling Performance. *J. Power Sources* **2002**, *112*, 606−613.

(11) Dubarry, M.; Qin, N.; Brooker, P. Calendar Aging of Commercial Li-Ion Cells of Different Chemistries − A Review. *Curr. Opin. Electrochem.* **2018**, 106−113.

(12) Leng, F.; Tan, C. M.; Pecht, M. Effect of Temperature on the Aging Rate of Li Ion Battery Operating above Room Temperature. *Sci. Rep.* **2015**, *5*, No. 12967.

(13) Yang, X.-G.; Zhang, G.; Ge, S.; Wang, C.-Y. Fast Charging of Lithium-Ion Batteries at All Temperatures. *Proc. Natl. Acad. Sci. U.S.A.* **2018**, *115*, 7266−7271.

(14) Li, Y.; Qian, K.; He, Y.-B.; Kaneti, Y. V.; Liu, D.; Luo, D.; Li, H.; Li, B.; Kang, F. Study on the Reversible Capacity Loss of Layered Oxide Cathode during Low-Temperature Operation. *J. Power Sources* **2017**, *342*, 24−30.

(15) Matadi, B. P.; Geniès, S.; Delaille, A.; Chabrol, C.; de Vito, E.; Bardet, M.; Martin, J.-F.; Daniel, L.; Bultel, Y. Irreversible Capacity Loss of Li-Ion Batteries Cycled at Low Temperature Due to an Untypical

https://dx.doi.org/10.1021/acs.jpcc.0c09972
J. Phys. Chem. C XXXX, XXX, XXX−XXX

Layer Hindering Li Diffusion into Graphite Electrode. *J. Electrochem. Soc.* **2017**, *164*, A2374.
(16) Zinth, V.; von Lüders, C.; Hofmann, M.; Hattendorff, J.; Buchberger, I.; Erhard, S.; Rebelo-Kornmeier, J.; Jossen, A.; Gilles, R. Lithium Plating in Lithium-Ion Batteries at Sub-Ambient Temperatures Investigated by in Situ Neutron Diffraction. *J. Power Sources* **2014**, *271*, 152−159.
(17) Ouyang, M.; Chu, Z.; Lu, L.; Li, J.; Han, X.; Feng, X.; Liu, G. Low Temperature Aging Mechanism Identification and Lithium Deposition in a Large Format Lithium Iron Phosphate Battery for Different Charge Profiles. *J. Power Sources* **2015**, *286*, 309−320.
(18) Taniguchi, S.; Shironita, S.; Konakawa, K.; Mendoza-Hernandez, O. S.; Sone, Y.; Umeda, M. Thermal Characteristics of 80 °C Storage-Degraded 18650-Type Lithium-Ion Secondary Cells. *J. Power Sources* **2019**, *416*, 148−154.
(19) Fathi, R.; Burns, J. C.; Stevens, D. A.; Ye, H.; Hu, C.; Jain, G.; Scott, E.; Schmidt, C.; Dahn, J. R. Ultra High-Precision Studies of Degradation Mechanisms in Aged LiCoO2/graphite Li-Ion Cells. *J. Electrochem. Soc.* **2014**, *161*, A1572−A1579.
(20) Dees, D. W.; Kawauchi, S.; Abraham, D. P.; Prakash, J. Analysis of the Galvanostatic Intermittent Titration Technique (GITT) as Applied to a Lithium-Ion Porous Electrode. *J. Power Sources* **2009**, *189*, 263−268.
(21) Weppner, W.; Huggins, R. A. Determination of the Kinetic Parameters of Mixed-Conducting Electrodes and Application to the System Li3Sb. *J. Electrochem. Soc.* **1977**, *124*, 1569.
(22) Cabañero, M. A.; Boaretto, N.; Röder, M.; Müller, J.; Kallo, J.; Latz, A. Direct Determination of Diffusion Coefficients in Commercial Li-Ion Batteries. *J. Electrochem. Soc.* **2018**, *165*, A847.
(23) Yang, H.; Bang, H. J.; Prakash, J. Evaluation of Electrochemical Interface Area and Lithium Diffusion Coefficient for a Composite Graphite Anode. *J. Electrochem. Soc.* **2004**, *151*, A1247.
(24) Levi, M. D.; Aurbach, D. Diffusion Coefficients of Lithium Ions during Intercalation into Graphite Derived from the Simultaneous Measurements and Modeling of Electrochemical Impedance and Potentiostatic Intermittent Titration Characteristics of Thin Graphite Electrodes. *J. Phys. Chem. B* **1997**, *101*, 4641−4647.
(25) Zhang, B.; Metzger, M.; Solchenbach, S.; Payne, M.; Meini, S.; Gasteiger, H. A.; Garsuch, A.; Lucht, B. L. Role of 1,3-Propane Sultone and Vinylene Carbonate in Solid Electrolyte Interface Formation and Gas Generation. *J. Phys. Chem. C* **2015**, *119*, 11337−11348.
(26) Dahn, J. R. Phase Diagram of Li X C 6. *Phys. Rev. B: Condens. Matter Mater. Phys.* **1991**, *44*, 9170.
(27) Levi, M. D.; Wang, C.; Markevich, E.; Aurbach, D.; Chvoj, Z. Noteworthy Electroanalytical Features of the Stage 4 to Stage 3 Phase Transition in Lithiated Graphite. *J. Solid State Electrochem.* **2003**, *8*, 40−43.
(28) Levi, M. D.; Wang, C.; Aurbach, D.; Chvoj, Z. Effect of Temperature on the Kinetics and Thermodynamics of Electrochemical Insertion of Li-Ions into a Graphite Electrode. *J. Electroanal. Chem.* **2004**, *562*, 187−203.
(29) Konz, Z. M.; McShane, E. J.; McCloskey, B. D. Detecting the Onset of Lithium Plating and Monitoring Fast Charging Performance with Voltage Relaxation. *ACS Energy Lett.* **2020**, *5*, 1750−1757.
(30) Fear, C.; Adhikary, T.; Carter, R.; Mistry, A. N.; Love, C. T.; Mukherjee, P. P. In Operando Detection of the Onset and Mapping of Lithium Plating Regimes during Fast Charging of Lithium-Ion Batteries. *ACS Appl. Mater. Interfaces* **2020**, *12*, 30438−30448.
(31) Amatucci, G. G.; Tarascon, J. M.; Klein, L. C. CoO_2, The End Member of the Li_xCoO_2 Solid Solution. *J. Electrochem. Soc.* **1996**, *143*, 1114.
(32) Finegan, D. P.; Quinn, A.; Wragg, D. S.; Colclasure, A. M.; Lu, X.; Tan, C.; Heenan, T. M. M.; Jervis, R.; Brett, D. J. L.; et al. Spatial Dynamics of Lithiation and Lithium Plating during High-Rate Operation of Graphite Electrodes. *Energy Environ. Sci.* **2020**, *13*, 2570−2584.
(33) Yao, K. P. C.; Okasinski, J. S.; Kalaga, K.; Shkrob, I. A.; Abraham, D. P. Quantifying Lithium Concentration Gradients in the Graphite Electrode of Li-Ion Cells Using Operando Energy Dispersive X-Ray Diffraction. *Energy Environ. Sci.* **2019**, *12*, 656−665.
(34) Cañas, N. A.; Einsiedel, P.; Freitag, O. T.; Heim, C.; Steinhauer, M.; Park, D. W.; Friedrich, K. A. Operando X-Ray Diffraction during Battery Cycling at Elevated Temperatures: A Quantitative Analysis of Lithium-Graphite Intercalation Compounds. *Carbon* **2017**, *116*, 255−263.
(35) Bauer, M.; Wachtler, M.; Stöwe, H.; Persson, J. V.; Danzer, M. A. Understanding the Dilation and Dilation Relaxation Behavior of Graphite-Based Lithium-Ion Cells. *J. Power Sources* **2016**, *317*, 93−102.
(36) Dees, D. W.; Rodrigues, M.-T. F.; Kalaga, K.; Trask, S. E.; Shkrob, I. A.; Abraham, D. P.; Jansen, A. N. Apparent Increasing Lithium Diffusion Coefficient with Applied Current in Graphite. *J. Electrochem. Soc.* **2020**, *167*, No. 120528.
(37) Logan, E. R.; Dahn, J. R. Electrolyte Design for Fast-Charging Li-Ion Batteries. *Trends Chem.* **2020**, *2*, 354−366.

https://dx.doi.org/10.1021/acs.jpcc.0c09972
J. Phys. Chem. C XXXX, XXX, XXX−XXX